Chinese Chemical Letters 33 (2022) 133–140

Contents lists available at ScienceDirect

Chinese Chemical Letters

journal homepage: www.elsevier.com/locate/cclet

Silicon-substituted rhodamines for stimulated emission depletion fluorescence nanoscopy

Ning Wang[a,1], Yumeng Hao[b,1], Xiaowei Feng[a], Haidan Zhu[a], Dazhi Zhang[b], Ting Wang[b,*], Xiaoyan Cui[a,*]

[a] Department of Chemistry, School of Chemistry and Molecular Engineering, East China Normal University, Shanghai 200241, China
[b] Department of Organic Chemistry, College of Pharmacy, Naval Medical University (Second Military Medical University), Shanghai 200433, China

ARTICLE INFO

Article history:
Received 26 April 2021
Revised 22 June 2021
Accepted 28 June 2021
Available online 2 July 2021

Keywords:
Silicon
Xanthene
Super-resolution
Stimulated emission depletion

ABSTRACT

As an essential part in the toolbox of super-resolution microscopy, stimulated emission depletion (STED) nanoscopy has been widely explored in revealing the substructure and bioactivities in fluorescence imaging. Among the applied STED fluorophores, silicon-substituted rhodamines (SiRs) belong to one of the most extensively employed fluorophores. The carboxy-SiR was favored in STED bioimaging with many advantages, including reliable photostability, cell permeability, tunable fluorogenicity, feasible structural decoration and so on. We reviewed the research of carboxy-SiR in the STED nanoscopy and hopefully this can inspire more efforts in the design and application of STED fluorophores.

1. Introduction

Overcoming the diffraction-limitation, a physical barrier that restricts the optical resolution to about 200 nm in conventional optical microscopy, super-resolution microscopy (SRM) has become one of the most versatile and powerful imaging techniques over the past two decades [1]. With the potential to reveal the complexity in subcellular structures, and subcellular localization or interaction of components in signaling networks with sub-diffraction resolution, SRM was widely explored in monitoring the biostructures and activities in complex biosystems. Various SRM techniques have been developed to generate super-resolution images, including stimulated emission depletion nanoscopy (STED) [2,3], structured illumination microscopy (SIM) [4,5], reversible saturable optical linear fluorescence transitions (RESOLFT), and single-molecule localization techniques, including ground-state depletion microscopy (GSD) [6], stochastic optical reconstruction microscopy (STORM) [7], and photo-activated localization microscopy (PALM) [8]. More techniques are recently developed for SRM, such as MINFLUX nanoscopy [9], expansion microscopy (U-ExM) [10].

Generally, imaging of the microstructures by most of these SRM techniques requires labeling of the specific molecules or structures with staining approaches, typically fluorescent strategies using fluorophores. SRM techniques can improve resolution beyond the diffraction limit by transferring the fluorophores that reside within the same diffraction-limited region into at least two distinguishing states, such as different temporal, spectral [11] or bright of fluorescence, which allows sequential recording of the fluorescent signals from the samples with size smaller than the diffraction limit [12]. Thus, the success of the SRM heavily relies on the properties of the probes, and different techniques have distinct requirements for the fluorescent probes. The central role of the fluorophores has been widely recognized in SRM techniques, and growing efforts have been devoted to developing SRM fluorescent probes. These fluorescent probes with fine-tuned structures and properties have boosted the application and further promoted the development and enthusiasm of SRM.

Among the commercialized SRM techniques, STED has been widely explored as a technique that can generate super resolution images directly from the recorded raw data without additional computation for the reconstruction of final images [13]. In STED nanoscopy, coaligned with the excitation laser, the depletion laser (called STED laser) is spatially patterned as a donut shape with zero intensity in the center region (Scheme 1a). Both lasers are on and the fluorophores are excited from ground state to excited state in the STED experiment. The fluorophores in the middle of the donut spontaneously emitted photons as a normal fluorescent process. However, fluorophores located in the donut region got de-excited by the excitation laser via the stimulated emission. As a re-

* Corresponding authors.
E-mail addresses: wangting1983927@gmail.com (T. Wang), xycui@chem.ecnu.edu.cn (X. Cui).
[1] These authors contributed equally to this work.

https://doi.org/10.1016/j.cclet.2021.06.075
1001-8417/

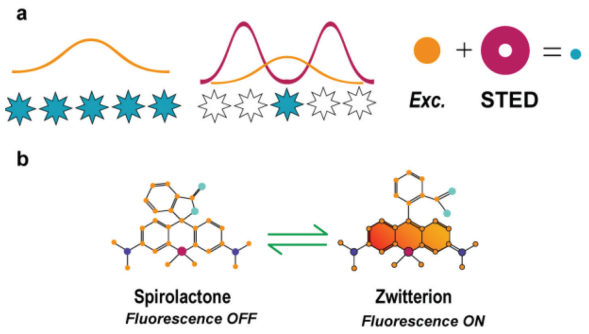

Scheme 1. Carboxy-SiR in STED nanoscopy. (a) Diagrammatic illustration of STED principle. An exciting laser (orange) light will excite all fluorophores (blue pentacles). When the depletion laser (dark red) of a donut shape with zero intensity in the center region was on, only few fluorophores located in the center of the donut can emit photons as a normal fluorescent process, making spatially resolve on the nanoscale possible. (b) The equilibrium and related change in fluorescence between the spirolactone form (fluorescence OFF) and zwitterion form (fluorescence ON) in the carboxy-SiR. For interpretation of the references to color in this figure legend, the reader is referred to the web version of this article.

sult, sub-diffraction spatial resolution was directly achieved in the very center of the donut by scanning of the two coaligned lasers together.

For qualified STED fluorophores, substantial photostability and efficient conversion between the depleted and excited states are essential for complete de-excitation without photobleaching [14]. Since the invention of STED in 1994 [3], especially the last 10 years, developing fluorophores that meets the high requirement of STED nanocopy has attracted extensive attentions, and many research groups have significant contribution to the family of STED fluorophores. Currently, organic fluorophores are predominantly applied in STED, among which silicon-substituted rhodamine (SiR) [15,16] belongs to one of the most widely used STED fluorophores.

In 2008, Xiao and Qian *et al.* pioneeringly reported the first SiR by the substitution of the bridging oxygen atom with a silicon atom in the rhodamine scaffold [17]. This work has been recognized as a breakthrough in the development of organic fluorophores, and this unique design strategy has further boosted the development of fluorophores and the SRM techniques. The designed SiR has inherited the excellent characters of rhodamine family as an outstanding fluorescent scaffold. Moreover, the perturbation of silicon has affected the electronic structures of SiR and resulted in distinctive physicochemical properties, including changed solubility, bathochromically shifted spectra, enhanced stability, and so on.

Uniquely, in rhodamine family, the regulation of fluorescence can be achieved by the spirocyclization for rhodamines, mainly carboxy-rhodamines with spiro-rings. Tuning the equilibrium (Scheme 1b) between the spirolactone form (closed derivative, L form, fluorescence OFF) and zwitterion form (opened derivative, Z form fluorescence ON) has been one of the most efficient and unique strategies for regulating the fluorescence in rhodamine family [18,19]. The L-Z equilibrium constant ($K_{L\text{-}Z}$) is the key for the fluorogenicity of rhodamines. For qualified spirolactam-rhodamine probes, they exist as the nonfluorescent form in aqueous solution, while after binding to targets, the equilibrium shifted into the Z form and resulted in strong fluorescence.

After the introduction of a silicon atom into the skeleton of xanthene core, the reduced electron density of the xanthene core has significantly shifted the L-Z equilibrium towards the L form and lowered the $K_{L\text{-}Z}$ in carboxy-SiR in aqueous solution. The efficiently locked spirolactam has depressed the background fluorescence and resulted in the sharp contrast between the nonfluorescent L form and fluorescent Z form, ensured excellent sensitivity and signal to noise ratio (SNR) [20,21]. The improved hydrophobicity in SiR has also enhanced its cellular permeability and optimized its performance in bioimaging. Far-red excitation and emission spectra of the SiR minimize the phototoxic effects during the STED imaging. Extremely reliable stability of SiR scaffold has ensured the reliable depletion in STED imaging process. These features well meet the requirement of STED nanoscopy and ensured the carboxy-SiRs one of the most widely applied STED fluorophores up to now. In this review, we focus on the progress in the application of carboxy-SiR in the STED nanoscopy.

2. STED with tuning the optical properties of carboxy-SiR

Despite SiR belongs to one of the most promising fluorescent scaffolds for STED imaging, the versatility of carboxy-SiR in sophisticated biological imaging experiments are urgently calling for more fluorophores with improved or specific properties. Lots of efforts are devoted to modulating the physicochemical properties of fluorophores. Recently, SiR with enhanced brightness and tuned L-Z equilibrium during bioimaging with finely tuned spectra have achieved by their structural modification. The progress has further prospered the application of SiR in fluorescence microscopy, especially in SRM.

2.1. Modification of the alkylamino moieties

Structural modification of the amino groups in rhodamine has been considered as one of the most efficient strategies for fine tuning the chemical-optical properties of rhodamines. The brightness, photostability, emission spectra, and the L-Z equilibrium can be efficiently tuned through the alkylamino moieties.

2.1.1. Enhanced brightness

It has been widely accepted for long time that reducing the structural flexibility of fluorophores can improve their fluorescence quantum yield [22]. In rhodamine family, the flexible (di)alkylamino substituents facilitate the internal rotation of the alkylamino groups and electron transfer from the (di)alkylamino substituent to the xanthene core. The related transition into twist intramolecular charge transfer (TICT) excited states of the fluorophores has increased the propensity to undergo nonradiative decay and eventually reduced the fluorescence quantum yield. Thus, decrease the flexibility of the amino groups by lowering the degrees of substitution or prevent the rotation of amino groups by cyclization can improve the fluorescence quantum yield of rhodamine. Three membered aziridine ring [23], four membered azetidine ring [24], and bridged 7-azabicyclo[2.2.1]heptyl substituents [25] are respectively introduced by Liu and Xu, Lavis, and Foley *et al.* to substitute the freely rotating *N,N*-dimethylamino groups for rigid structures with enhanced brightness and photostability in classical rhodamines. We will mainly focus on the structural modification and related properties of SiR in this review.

Lavis *et al.* have turned the *N,N*-dimethylamino groups in SiR, rhodamines, and coumarins into four-membered azetidine rings. This strategy has improved the brightness and photostability of fluorophores while preserving their spectral properties and cell permeability. The addition of two carbon atoms have restricted the rotation of the flexible *N,N*-dimethylamino groups and resulted in enhanced fluorescence quantum yield. Taking one of the representative fluorophores, Janelia Fluor646 (JF_{646}, Fig. 1), the derivative of SiR as an example, the incorporation of azetidine groups has bathochromically shifted the spectra of JF_{646} with improved fluorescence quantum yield ($\lambda_{abs}/\lambda_{em}$ = 646 nm/664 nm, Φ = 0.54) [24]. This structural modification approach has been recognized as a generalizable strategy for improving the fluorescence quantum yield of fluorophores.

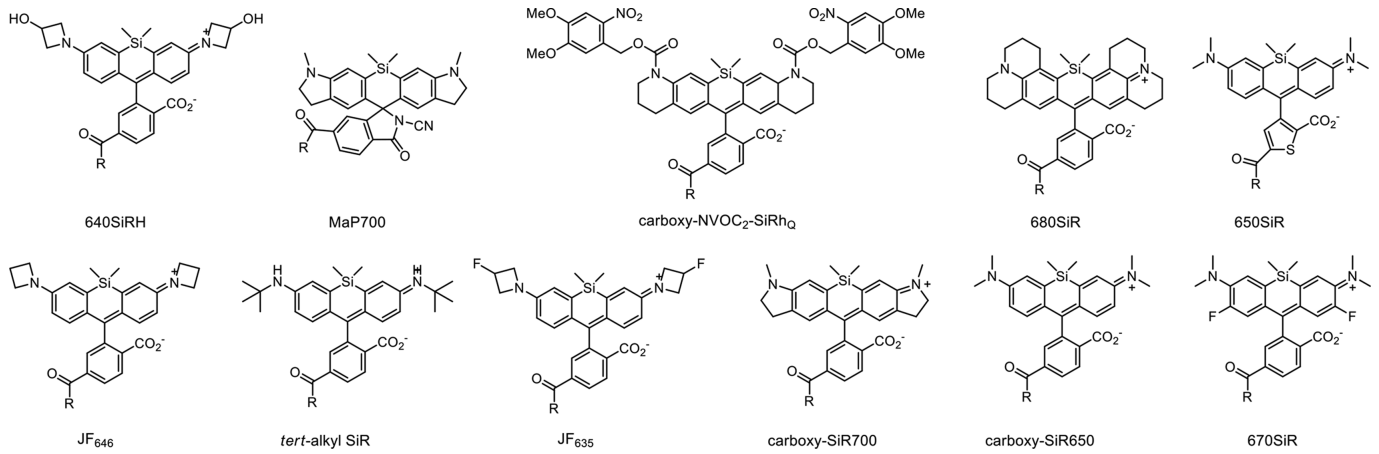

Fig. 1. Structures of carboxy-SiR derivatives.

2.1.2. Improved stability

STED imaging has high requirement for the stability of probes owing to the simultaneously irritation of two powerful laser pulses during the SRM experiments. Usually, the strategy for enhancing the brightness of SiRs by the elimination of TICT also contributed to the improvement of their photostability by reducing the structural flexibility and improving the photoconversion-resistant.

Hell *et al*. have recently pointed out that modification of the alkyamino moieties can also improve the photostability of SiR by stabilizing the spectral of fluorescence labels. The spectral stability is critical for robust results in SRM bioimaging. Introducing electron-withdrawing groups, such as 2,2,2-trifluoroethyl as amine substituents, unsubstituted amino, and tert–alkyl substituents lacking α-hydrogen atoms in the amino moieties (*tert*–alkyl SiR, Fig. 1) are efficient approaches to eliminate the photooxidative and enhance the photostability of the probes [26]. STED imaging was achieved by the Halo-tagged analog of SiR in living cells.

2.1.3. Tuning the spectra

Rational tuning the spectra of fluorophores are crucial for the design of probes with desired properties. It has been confirmed that the incorporation of azetidine groups with different substitutes can precisely tune the spectral and chemical properties of rhodamines. After the introduction of a single fluorine atom on each azetidine ring in fluorophore JF_{646}, a 13 nm hypsochromic shift was observed in the resulted probe Janelia Fluor635 (JF_{635}, Fig. 1) [27]. Compared with JF_{646}, the hydroxylated analog of JF_{646} (640SiRH, Fig. 1) has slightly red-shifted spectra ($\lambda_{abs}/\lambda_{em}$ = 641 nm/662 nm, Φ = 0.56) [28].

Introducing an indoline into the SiR scaffold results in the 50 nm bathochromically shifted excitation and emission maxima, from carboxy-SiR650 (Fig. 1) to carboxy-SiR700 (Fig. 1) [29]. By incorporation of conformationally rigid julolidine core in SiR, the bis-julolidine-fused analog of SiR, 680SiR was applied in STED with bathochromically shifted spectra ($\lambda_{abs}/\lambda_{em}$ = 679 nm/697 nm, Φ = 0.42) [30].

2.1.4. Tuning the L-Z equilibrium

One of the most remarkable features of SiR is the relatively lowered $K_{L\text{-}Z}$ after the incorporation of a silicon atom. Thus, in aqueous solution, the SiR-based probes are dominant in the nonfluorescent, lipophilic form, ensured highly cellular permeability and low background signals. After binding to the targets, the equilibrium shifted into the fluorescent zwitterion form, yielding strong fluorescence.

Lavis *et al*. have extensively explored the Janelia Fluor dyes and proved that there is reciprocal relationship between the $K_{L\text{-}Z}$ and fluorogenicity. In SiR probes, tuning the $K_{L\text{-}Z}$ between 10^{-2} and 10^{-3} gives ligands with fluorogenicity of about 5–10 folds. Different approaches are attempted for lowering the $K_{L\text{-}Z}$, including replacement of the *N,N*-dimethylamino groups into azetidine rings, further fluorinating the azetidine rings or the xanthene structures [31].

After the introduction of fluorine atoms, the lowered $K_{L\text{-}Z}$ indicating that the L-Z equilibrium of JF_{635} shifted into the non-fluorescent lactone form and resulted in extremely low background fluorescence [27]. The Halo-tag conjugated JF_{635} has exceptionally low background and high SNR in STED bioimaging. Differently, the hydroxylated analog of JF_{646}, 640SiRH undergoes ring opening process and exists predominantly in the fluorescent zwitterionic forms in environment with high water content [28].

2.1.5. Photoactivatable probes

Photoactivatable probes are extensively applied in bioimaging, however, STED imaging with photoactive probes is changeling, owing to the potentially unwanted activation by the powerful STED laser. Modification of alkylamino moieties with photoactive group, *ortho*-nitrobenzyl (ONB) carbamate, has resulted in excellent photoactivated probes (carboxy-$NVOC_2$-$SiRh_Q$ Fig. 1) for STED bioimaging of actin filaments in HeLa cells [32].

2.2. Modification of the xanthene core, benzyl, and carboxy structure

Modification of the xanthene cores in SiR has also been recognized as an important approach for tuning the properties of the related probes. Introduction of electron-withdrawing groups into the xanthene core, such as fluorine atoms, can significantly reduce the electron density of xanthene core and shift the L-Z equilibrium towards the L form [20,33]. For example, conjugating two fluorine atoms into the xanthene skeleton has resulted in bathochromically shifted spectra and shifted L-Z equilibrium in 670SiR (Fig. 1, $\lambda_{abs}/\lambda_{em}$ = 670 nm/696 nm, Φ = 0.03) [33]. However, introducing the fluorine atoms in SiR also leads to decreased fluorescence quantum yield.

Other than modification of the xanthene ring system, structural decoration of the benzene ring can also affect the L-Z equilibrium. Replacement of the benzene ring with thiophene ring can slightly bathochrmically shift the spectra, as demonstrated in 650SiR (Fig. 1, $\lambda_{abs}/\lambda_{em}$ = 650 nm/672 nm, Φ = 0.36). However, the formation of colorless L form is less favored in the 650SiR than SiR, owing to the increased angle strain from the formation of five-membered lactone fused to the five membered thiophene ring [33].

In the structural modification of rhodamine and SiR, installing an amide group next to the carboxy group can stabilize the fluorophore in the non-fluorescent, spirolactone state through the

neighboring group effect. Thus, the stabilized hydrophobic L form significantly enhanced the cellular permeability and reduced the background fluorescence, facilitating their STED bioimaging. Although the neighboring group effect is more significant in less hydrophobic rhodamine, this strategy still provides an efficient and simple approach for tuning the performance of SiRs [34].

Recently, Johnsson and Wang *et al.* have reported a general strategy to tune the cell permeability and fluorogenicity of rhodamine and substituted rhodamine without changing their spectroscopic properties by replacing the carboxy groups with different functional amides. In SiR, acyl cyanamide was introduced into SiR (MaP700, Fig. 1) and resulted in fluorophores with excellent cell permeability and fluorogenicity [20]. The designed MaP700-Halo probe was applied in live-cell STED nanoscopy.

3. STED by carboxy-SiR with different targeting strategies

In SRM imaging, the sub-diffraction resolution of complex cellular processes and structures can be visualized through the spatially distinguishable fluorescent reporters. Various strategies have been designed for fluorescent probes that can specifically label the finite structures, accompanied with strong fluorescence in biosystems. Usually, the specific location of the fluorescence in the probes is achieved through attaching the targeting groups to the fluorophores. Different targeting strategies are applied in STED by carboxy-SiR.

3.1. Labeling through the genetically encoded markers

After the wide application of fluorescent proteins, many attentions have been devoted to labeling proteins through genetic fusion. Taking advantage of the flexibility and reliable optical properties of chemical probes, various strategies have been developed for specifical labeling of proteins with synthetic probes. In these methods, a genetically encoded protein tag, which can be covalently labeled with a small molecule/functional group, is fused to the protein of interest (POI). Different protein tags are used for covalently labeling in living cells, among which the SNAP-tag, Halo-tag, and CLIP-tag are extensively applied in STED.

SNAP-tag is derived from the 20 kDa DNA repair protein O^6-benzylguanine alkyltransferase (AGT) and can be covalently recognized by O^6-benzylguanine (BG) derivatives. CLIP-tag is a modified version of SNAP-tag. It is also derived from human O^6-alkylguanine alkyltransferase, instead of benzyguanine, CLIP-tag can react with benzylcytosine (BC) derivatives [35]. Halo-tag is designed with a modified bacterial haloalkane dehalogenase (a 33.6 kDa protein), which can covalently recognize the chloroalkane linker [36]. These protein tags undergo irreversible reactions with reliable sensitivity and speed with the recognition groups, which are feasible for synthesis and chemical decoration. Fluorescent probes with designed recognition groups are extensively applied in covalently modify proteins and transfer the fluorophores through the specific reaction with these protein tags. The organic fluorophores labeled proteins bearing superior brightness, photostability and flexibility, well meets the requirement of STED imaging.

The chemical modification of SiR with protein tags have ensured both the feasible tuning of fluorescence through the skeleton of carboxy-SiR and high specification of protein tags. In 2013, K. Johnsson and *et al.* have developed the carboxy-SiR650 (Fig. 2) with SNAP, CLIP, and Halo-tag labeling in bioimaging. The reliable fluorescence triggering strategy in carboxy-SiR through the spiroring has ensured strong fluorescence of high SNR in bioimaging, even without washing steps. They have also successfully applied the carboxy-SiR-SNAP in the STED imaging of the living cells with SNAP-tag fusion proteins of histone H2B and centrosomal protein

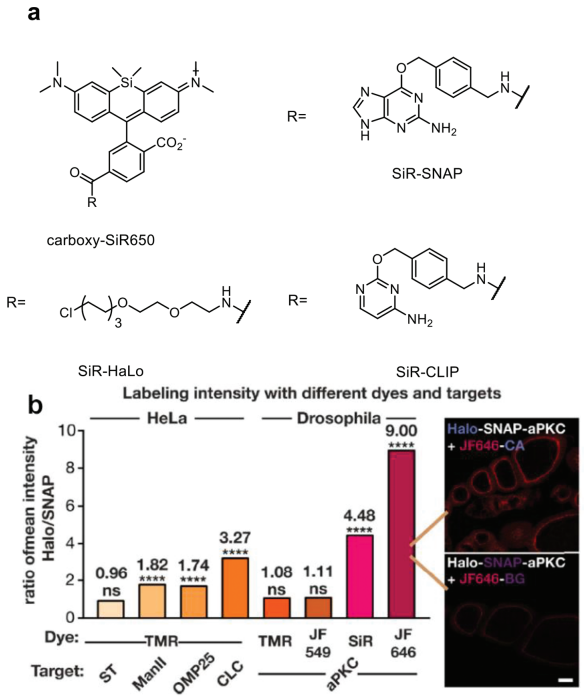

Fig. 2. SiR with genetically encoded markers: (a) SiR-SNAP, SiR-Halo, and SiR-CLIP. (b) Comparison of Halo and SNAP-tag labeling with TMR, JF_{549}, SiR, and JF_{646} in HeLa cells and Drosophila egg chambers. Scale bar: 20 mm. Copied with permission [38]. Copyright 2019, Erdmann *et al.*

Cep41, respectively [37]. For living U2OS cells labelled with the SiR-SNAP through the SNAP-Cep41, dynamic of the microtubules was vividly tracked. Moreover, the ring-like structure along the axis of the centriole was directly visualized in the STED images. In the SNAP-Cep41 labelled centriole, both the diameter and length of the hollow centriole captured by STED are consistent with data obtained by other techniques. This is the first time for the visualization of centrosomal proteins in living cells with microscopy of ultra-high spatial resolution. The excellent photophysical properties of SiR makes it a powerful tool for STED bioimaging with excellent spatial and temporal resolution.

Taking advantage of the highly specific molecular recognition between the genetically encoded proteins and the related protein-tags, SiR fused with Halo (SiR-Halo, Fig. 2a) was applied in evaluating the spatial distribution of synapse proteins for unveiling the mechanisms of synaptic transmission *in vivo*. The transgenic knock-in mouse line engineered to express endogenous postsynaptic density 95 (PSD95) protein in fusion with the HaloTag enzyme, which allowed covalently labeling of the PSD95 with probe SiR-Halo [39]. Using an upright STED nanoscopy, the diversity of PSD95 scaffold was characterized with high contrast and low background *in vivo*. The nanoscale distribution of the abundant scaffolding protein PSD95 at the postsynaptic membrane of excitatory synapses was resolved with lateral resolution down to ~70 nm in the visual cortex at $\leq$ 25-μm depth. With improved resolution, the experimental observation suggested that PSD95 mainly exists as large scaffold with complex internal organization, rather than isolated nanoclusters. Moreover, the relation of the PSD95 nanoscale morphology to the spin head shape was also observed and agreed with literature study by electron microscopes (EM). Small dendritic spines usually harbor small round PSD95 assemblies, while large spines contain complex-shaped PSD95 scaffolds [39].

The performance of protein tags is crucial in the STED imaging of finite structures with super resolution. It has been confirmed that different protein tags have distinct effects on the resulted

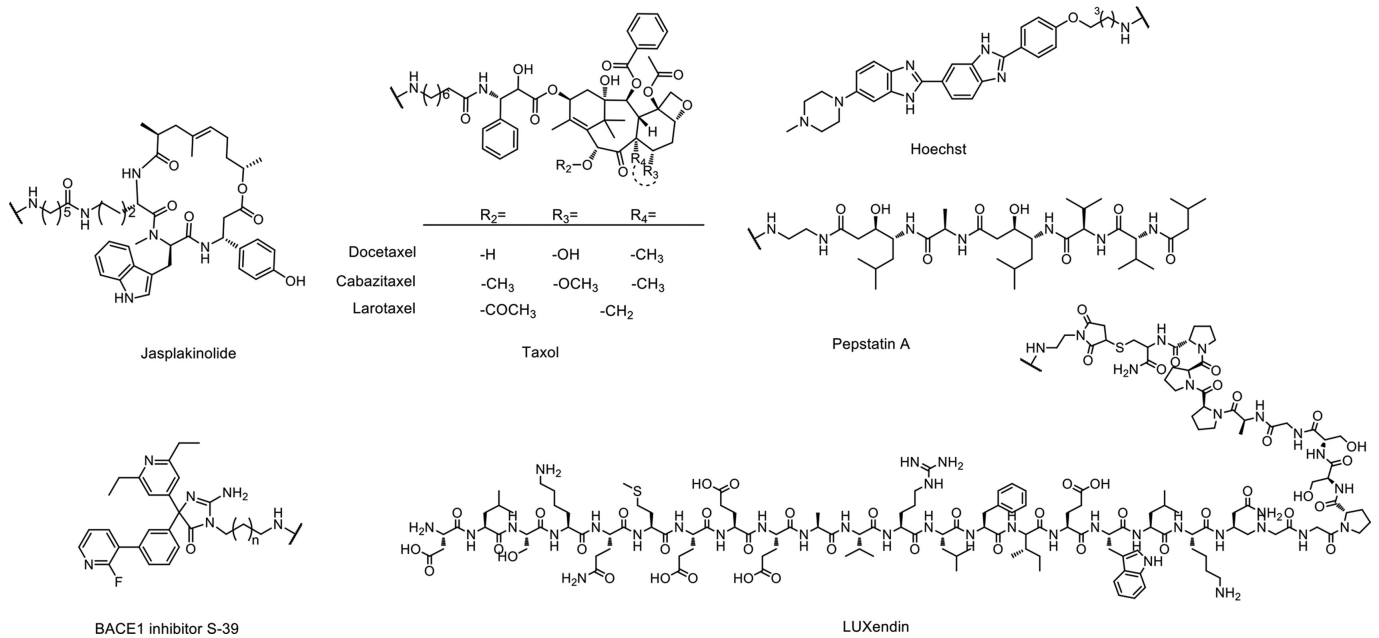

Fig. 3. Non-covalent targeting groups.

STED imaging. Carboxy-SiR was applied as the bright fluorescent reporter for quantitively systematic comparison of the SNAP and Halo-tagging strategies. Comparing with the fluorescence brightness, transfection efficiency, substrate permeability, expression levels of different protein tags, they have confirmed that Halo-tag is generally superior in STED nanoscopy. The fluorescent signals of SiR are about 9-fold higher (Fig. 2b) with Halo-tags than SNAP-tags [38]. Efforts have also been devoted to the improvement of the labeling groups. Researchers have reported that functionalize the SNAP-tag substrate BG with a charged sulfonate (SBG) can efficiently improve the extracellular labeling by SNAP-tag by reducing non-specific staining and related background noise. This have also provided a novel approach/aspect for improving the STED imaging with protein tags [40].

3.2. Labeling with targeting groups through the non-covalent recognition

The strong and specific non-covalent interaction between certain functional groups and related organelle organizations are one of the most widely applied strategies for staining biostructures with high specificity in living cells. Significantly, directly attaching the small molecular probes into the structure of interest may enhance the resolution substantially. Different ligands are attached to the scaffold of carboxy-SiR for STED imaging *in vivo*.

The antitumor drug, Taxol (paclitaxel) and its derivatives, were usually applied as the microtubule-stabilizing agents with high specificity to microtubule cytoskeletons in variety of cells [41]. SiR-tubulin [42] (carboxy-SiR650 with docetaxel group, Fig. 3), probe designed by the conjugation of SiR to the ligand docetaxel was applied in the analysis of microtubules by STED. Living human fibroblasts stained with SiR-tubulin have sketched the peripheral microtubules and the microtubules of the centrosome with extremely high spatial resolution (the apparent microtubule diameter was 39 ± 10 nm) [42]. SiR-tubulin was also applied in tracking the microtubule dynamics by STED. Apart from the functionalization of docetaxel, other derivatives of paclitaxel, including cabazitaxel and larotaxel were also evaluated after conjugation with SiR. The apparent microtubule diameter was 29 ± 11 nm with reduced background fluorescence by SiR-CTX (carboxy-SiR650 with cabazitaxel,

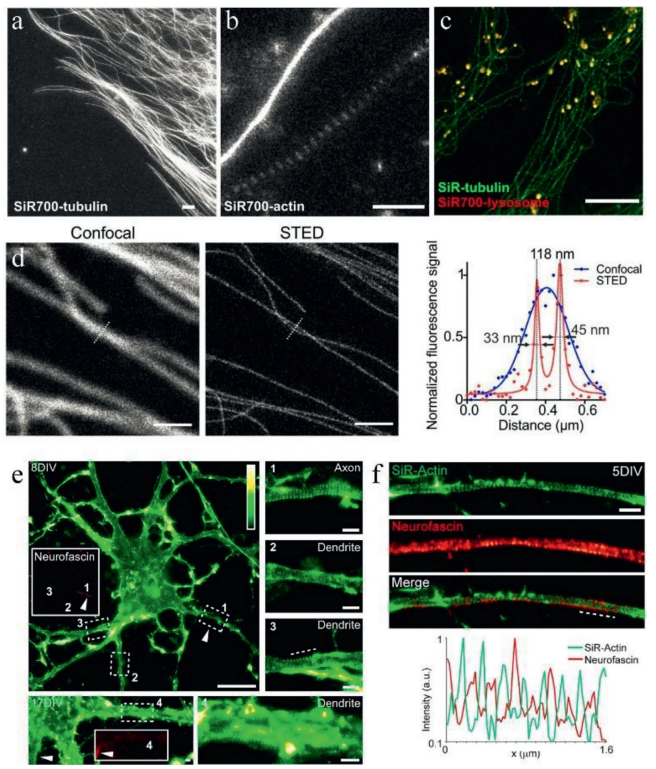

Fig. 4. SiR-tubulin and actin STED imaging. (a) Images of human primary fibroblasts stained with SiR700-tubulin. (b) STED images of primary rat hippocampal neurons stained with SiR700-actin probes. (c) Two-color STED nanoscopy of living human primary fibroblasts stained with SiR-tubulin (green) and SiR700-lysosome (red). Scale bars = 1 μm (a,b) and 5 μm (c). Copied with permission [29]. Copyright 2016, American Chemical Society. (d) Image of the muscle tissue stained with SiR-CTX. Scale bars = 1 μm. Copied with permission [43]. Copyright 2018, Royal Society of Chemistry. (e) STED images of living neurons. Scale bars = 10 μm for 8 DIV, and 1 μm for 17 DIV. (1–4) Close-ups of the regions indicated in the images of the neurons at 8 and 17 DIV. Scale bars = 1 μm. (f) STED image of a living hippocampal neuron. Scale bars = 1 μm. Copied with permission [45]. Copyright 2015, D'Este *et al*. For interpretation of the references to color in this figure legend, the reader is referred to the web version of this article.

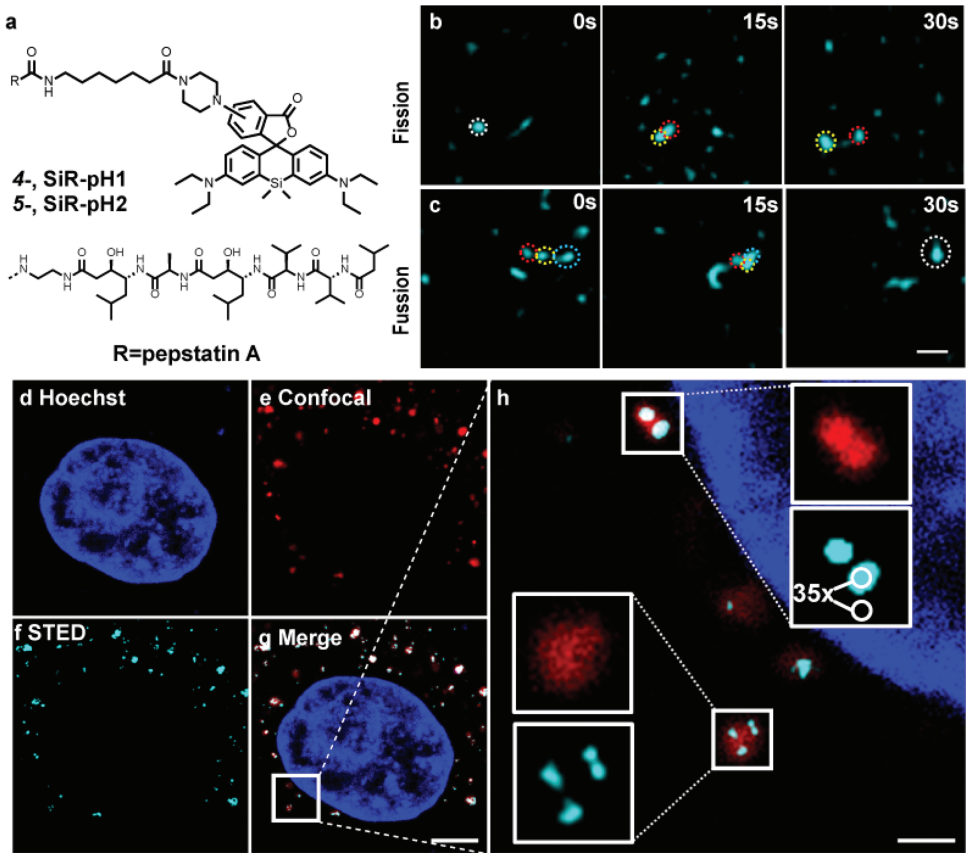

Fig. 5. Live STED imaging of lysosomes by SiR-pH2. (a) Structures of SiR-pHs; (b, c) fission and fusion of lysosomes, scale bar = 250 nm; (d, e) confocal imaging of nucleus labeled with Hoechst (blue) and lysosomes labeled with SiR-pH2 (red), scale bar = 25 μm; (f, g) STED imaging of lysosomes (cyan), scale bar = 25 μm; (h) enlarged images of selected regions in (g), scale bar = 1 μm. Copied with permission [48], Copyright 2021, Wiley-VCH. For interpretation of the references to color in this figure legend, the reader is referred to the web version of this article.

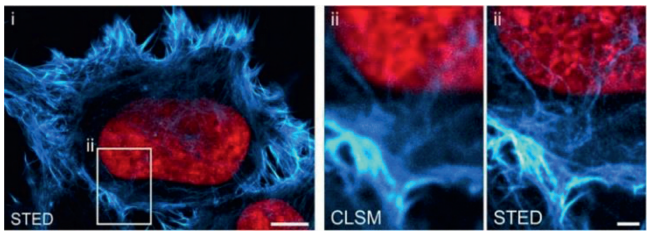

Fig. 6. Two-color 2D STED image of a fixed HeLa cell labeled for actin (lifeactAF594, cyan hot) and DNA (JF_{646}-Hoechst, red). Scale bars are 5 μm (i), 1 μm (ii). Copied with permission [52]. Copyright 2018, American Chemical Society. For interpretation of the references to color in this figure legend, the reader is referred to the web version of this article.

Fig. 3) [43], and the tubulin structure in muscle tissues were also vividly imaged with SiR-CTX (Fig. 4d).

Phalloidin and some other cyclic peptides, such as jasplakinolide, can specifically bind to actin filaments and stabilize their structures [44]. SiR-actin (carboxy-SiR650 with jasplakinolide, Fig. 3), in which SiR is chemically linked with desbromodesmethyl-jasplakinolide, a group with extremely high specificity to the F-actin filaments, was designed for locating the spatial arrangement of actin in primary rat hippocampal neurons. STED imaging of the stained neuron cells revealed periodic structures along the axons with a periodicity of about 180 nm [42].

The striking performance of SiR-actin in live cell STED nanoscopy has attracted more interests and further exploration. Hell *et al.* used STED live cell imaging and fluorescent probe SiR-actin for the ultrastructure of endogenous F-actin in living hippocampal neurons. Benefited from the ultrahigh resolution of STED, they have demonstrated that the periodic subcortical actin structure is present in both axons and dendrites with fluorescent probe SiR-actin (Fig. 4). The periodic pattern of cytoskeletal proteins was also observed in myelinated sciatic nerve fibers at the nodes of Ranvier. In living cells, they proved that the organization of cytosolic actin in patches and bundles is both evolving in time and spatially regulated [45].

SiR was employed in tracking β-site amyloid precursor protein (APP)-cleaving enzyme 1 (BACE1) for unveiling the pathogenesis aminohydantoin through S-39 (Fig. 3), an efficient and selective inhibitor of BACE1, was introduced into carboxy-SiR650 for a novel BACE1 labeling probe with high affinity, specificity, and fluorogenicity, SiR-BACE1. The vesicular distribution of overexpressed BACE1 was detailly visualized by the STED nanoscopy of SiR-BACE1 stained neuronal cell lines [46].

In tracking of cellular lysosome with high spatial resolution, a spherical, tiny membrane-bound vesicles with diameter about 100–500 nm, the powerful combination of SiR and STED has ensured monitoring the dynamic of lysosome *in vivo* through the specific recognition of pepstatin and lysosome [47]. Our group has recently successfully tracked the dynamic of lysosomal structure and pH by a dually fluorogenic strategy [48]. The designed probes SiR-pHs (Fig. 5) bearing both the pepstatin and H^+-receptor. Rather than tuning the L-Z equilibrium by the targets, the equilibrium is controlled by both the pH-trigged photoinduced electron transfer (PeT) mechanism and targeting protein. Thus, strong fluorescence only released in the existence of targeting protein and acidic lysosomal pH, offered precisely tracking the dynamic of lysosome in living cells by STED (Fig. 5). The dually fluorogenic features of the probes with a perfect mutual enhancement in sensitivity, speci-

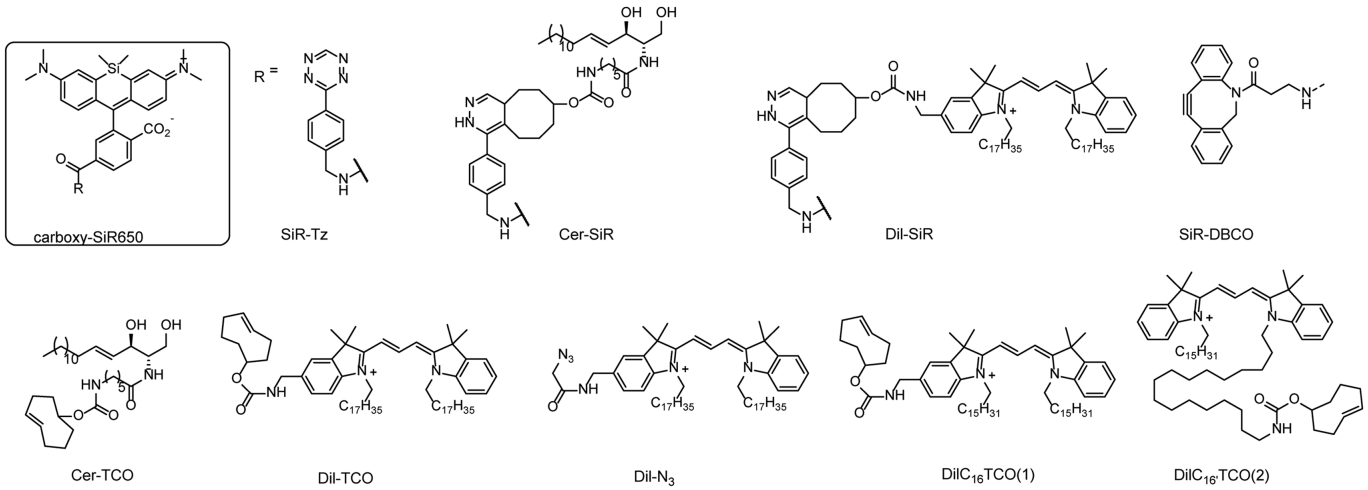

Fig. 7. HIDE probes and orthogonal reagent structures.

ficity, and spatial resolution has offered a novel approach for the design of fluorescent probes for SRM.

SiR was also applied in tracking the glucagon-like peptide-1 receptor (GLP1R), a class B G protein-coupled receptor (GPCR) involved in metabolism. The conjugation of SiR and a novel antagonistic scaffold (Fig. 3, LUXendin) to GLP1R yields probe LUXendin651. The nanoscopic characterization of endogenous GLP1R by STED both *in vitro* and *in vivo* have provided insight into the distribution and dynamics of class B GPCR [49].

Hoechst 33342 is a popular DNA minor groove-binder with minimal toxicity in living cells. Incorporation the bisbenzimide core of Hoechst 33342 and carboxy-SiR has provided SiR-Hoechst, an extremely powerful probe for the STED imaging of nucleus. The designed probe composed of Hoechst attached to the 6′-carboxy SiR. A recent study has revealed that the 5′-carboxy SiR is superior in STED imaging with increased brightness and lower cytotoxicity by conjugate the Hoechst 33258 to the SiR for nuclear staining [50,51]. High nuclear-staining specificity of SiR-Hoechst within both excitation and emission spectra in far-red region has ensured bioimaging of cellular nucleus with high SNR and low toxicity from the laser pulse. JF_{646}-Hoechst was used in imaging of the bacterial nucleoid and envelop by STED (Fig. 6) [52].

Telomere, segment of DNA containing sequence TTAGG and occurring at the ends of chromosomes in eukaryotic cells [53], was also monitored by SiR-based probe. In the probe, the SiR conjugated with a tandem tetramer pyrrole-imidazole polyamide, which targets 24 bp in the telomeric double stranded DNA to give the probe, SiR-TTet59B [54]. The structures and dynamic movements of telomeres were vividly observed in living cells by STED. Rather than DNA, Other nucleic acid, such as RNA was efficiently monitored by STED through the chemical modification of carboxy-SiR. SiRA, a carboxy-SiR based probe that can specifically bind to aptamer with extremely increased fluorescence (fluorescence quantum yield up to 0.98) was used to visualize the expression of RNA in bacteria *in vivo* by STED [55].

3.3. Bio-orthogonal labeling with HIDE

High-density environment-sensitive (HIDE) probes belong to a special group of lipid-based fluorescent probes. A set of HIDE probes are designed through the bio-orthogonal labeling strategy for the STED imaging of different subcellular structures using carboxy-SiR650. Two reagents are required for the specific targeting: a bright, reactive tetrazine-tagged fluorophore, for example, SiR-Tz (Fig. 6), and *trans*-cyclooctene containing ceramide lipid (Cer-TCO, Fig. 6), which can localize the membrane-permeable SiR within a lipophilic membrane environment. The two reagents underwent an extremely rapid reaction, tetrazine-click reaction, and assembled together into Cer-SiR *in cellulo*. The Cer-SiR specifically localized in Golgi with strong and endurable fluorescence suitable for STED [56]. DiI-TCO, a high-density lipid probe that specially localized to the plasma membrane, was readily reacted with SiR-Tz to form the HIDE probe DiI-SiR. The designed probe succeeded in long-time-lapse STED imaging of the dynamic of the plasma membrane in living cells [57].

Dual organelle dynamics was monitored by STED using a HIDE probe SiR-DBCO. The probe was assembled through the strain-promoted azide-alkyne cycloaddition (SPAAC) reaction between the azide in Dil-N_3 and the dibenzoazacyclooctyne (DBCO), which is covalently attached to SiR in SiR-DBCO. The two-component HIDE probes have ensured the long time-lapse two-color STED imaging of two organelles simultaneously [58].

The HIDE probes were also applied in tracking dynamic of endo-lysosomal membrane by STED. SiR-Tz, SiR bearing a tetrazine reaction partner, reacts with a reactive lipid-like molecule ($DiIC_{16}TCO$ (1) or $DiIC_{16'}TCO$ (2) structures show in Fig. 7) to form the HIDE probe for the acquisition of long time-lapse STED videos (Fig. 8) without detectable change in the organelle structure and function [59].

The HIDE probe ensured the quantitative analysis of the endosome dynamics and revealed the inter-endosome kiss-and-run events that cannot be resolved by confocal methods.

4. Summary

The outstanding optical properties, feasible labeling and fluorescence triggering strategies of carboxy-SiR have largely prospered the application of nanoscopy techniques. Especially, carboxy-SiR have been recognized as one of the most excellent STED fluorescent scaffolds with extensive application and great potential for further exploration. Hopefully the review of this representative group of fluorophores in the application of STED nanoscopy can bring some insight into the design and develop of STED fluorophores.

Declaration of competing interest

The authors declare that they have no known competing financial interests or personal relationships that could have appeared to influence the work reported in this paper.

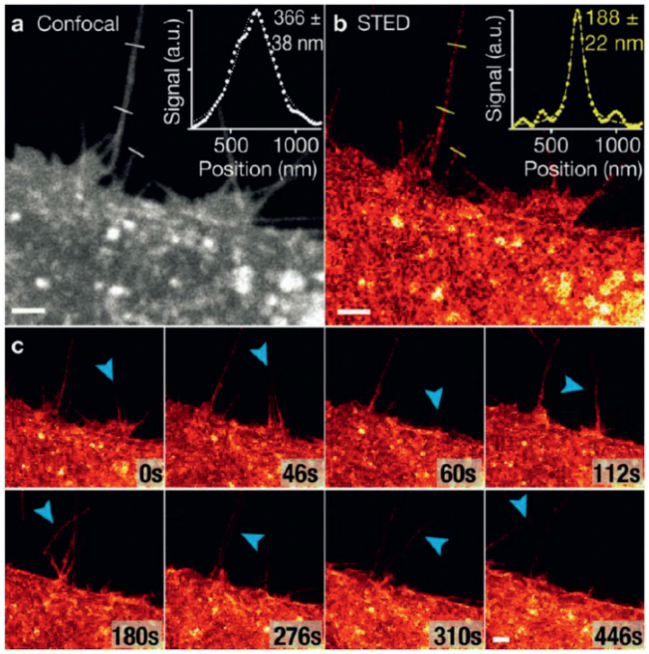

Fig. 8. Long-time-lapse STED imaging of live HeLa cells labeled with DiI-SiR. (a) Confocal image of filopodia. (b) STED image of filopodia. (c) Time-lapse images of HeLa cell dynamics. Blue arrows indicate filopodia movement. Scale bars: 2 mm. Copied with permission [57]. Copyright 2017, Wiley-VCH. For interpretation of the references to color in this figure legend, the reader is referred to the web version of this article.

Acknowledgments

This study was supported by the Natural Science Foundation of Shanghai (Nos. 19ZR1480000, 20ZR1470200), National Natural Science Foundation of China (No. 81830106), and the Program for Professor of Special Appointment (Eastern Scholar, No. TP2017039).

References

[1] M. Fernandez-Suarez, A.Y. Ting, Nat. Rev. Mol. Cell Biol. 9 (2008) 929–943.
[2] T.A. Klar, S.W. Hell, Opt. Lett. 24 (1999) 954–956.
[3] S.W. Hell, J. Wichmann, Opt. Lett. 19 (1994) 780–782.
[4] M.G. Gustafsson, Proc. Natl. Acad. Sci. U. S. A. 102 (2005) 13081–13086.
[5] X. Li, J. Zheng, W. Liu, et al., Chin. Chem. Lett. 31 (2020) 2937–2940.
[6] M. Kroug. S.W. Hell, Appl. Phys. B 60 (1995) 495–497.
[7] M.J. Rust, M. Bates, X. Zhuang, Nat. Methods 3 (2006) 793–795.
[8] S.T. Hess, T.P. Girirajan, M.D. Mason, Biophys. J. 91 (2006) 4258–4272.
[9] K.C. Gwosch, J.K. Pape, F. Balzarotti, et al., Nat. Methods 17 (2020) 217–224.
[10] T. Ku, J. Swaney, J.Y. Park, et al., Nat. Biotechnol. 34 (2016) 973–981.
[11] X. Zhang, L. Chen, Z. Huang, et al., Chem. Eur. J. 27 (2021) 3688–3693.
[12] S.W. Hell, Science 316 (2007) 1153–1158.
[13] H. Blom, J. Widengren, Chem. Rev. 117 (2017) 7377–7427.
[14] J. Li, M. Zhang, L. Yang, et al., Chin. Chem. Lett. (2021), doi:10.1016/j.cclet.2021.04.041.
[15] F. Deng, Z. Xu, Chin. Chem. Lett. 30 (2019) 1667–1681.
[16] Y. Xiao, X. Qian, Coord. Chem. Rev. 423 (2020) 213513.
[17] M. Fu, Y. Xiao, X. Qian, et al., Chem. Commun. (Camb.) (2008) 1780–1782.
[18] W. Chi, Q. Qi, R. Lee, et al., J. Phys. Chem. C 124 (2020) 3793–3801.
[19] W. Zhou, X. Fang, Q. Qiao, et al., Chin. Chem. Lett. 32 (2021) 943–946.
[20] L. Wang, M. Tran, E. D'Este, et al., Nat. Chem. 12 (2020) 165–172.
[21] F. Deng, Q. Qiao, J. Li, et al., J. Phys. Chem. B 124 (2020) 7467–7474.
[22] M. Vogel, W. Rettig, R. Sens, K.H. Drexhage, Chem. Phys. Lett. 147 (1988) 452–460.
[23] X. Liu, Q. Qiao, W. Tian, et al., J. Am. Chem. Soc. 138 (2016) 6960–6963.
[24] J.B. Grimm, B.P. English, J. Chen, et al., Nat. Methods 12 (2015) 244–250.
[25] X. Song, A. Johnson, J. Foley, J. Am. Chem. Soc. 130 (2008) 17652–17653.
[26] A.N. Butkevich, M.L. Bossi, G. Lukinavicius, S.W. Hell, J. Am. Chem. Soc. 141 (2019) 981–989.
[27] J.B. Grimm, A.K. Muthusamy, Y. Liang, et al., Nat. Methods 14 (2017) 987–994.
[28] A.N. Butkevich, V.N. Belov, K. Kolmakov, et al., Chem. Eur. J. 23 (2017) 12114–12119.
[29] G. Lukinavicius, L. Reymond, K. Umezawa, et al., J. Am. Chem. Soc. 138 (2016) 9365–9368.
[30] A.N. Butkevich, H. Ta, M. Ratz, et al., ACS Chem. Biol. 13 (2018) 475–480.
[31] Q. Zheng, A.X. Ayala, I. Chung, et al., ACS Cent. Sci. 5 (2019) 1602–1613.
[32] M. Weber, T.A. Khan, L.J. Patalag, et al., Chem. Eur. J. 27 (2021) 451–458.
[33] A.N. Butkevich, G.Y. Mitronova, S.C. Sidenstein, et al., Angew. Chem. Int. Ed. 55 (2016) 3290–3294.
[34] J. Bucevicius, G. Kostiuk, R. Gerasimaite, et al., Chem. Sci. 11 (2020) 7313–7323.
[35] A. Gautier, A. Juillerat, C. Heinis, et al., Chem. Biol. 15 (2008) 128–136.
[36] G.V. Los, L.P. Encell, M.G. McDougall, et al., ACS Chem. Biol. 3 (2008) 373–382.
[37] G. Lukinavicius, K. Umezawa, N. Olivier, et al., Nat. Chem. 5 (2013) 132–139.
[38] J.M. Masch, H. Steffens, J. Fischer, et al., Proc. Natl. Acad. Sci. U. S. A. 115 (2018) E8047–E8056.
[39] R.S. Erdmann, S.W. Baguley, J.H. Richens, et al., Cell Chem. Biol. 26 (2019) 584–592.
[40] P. Poc, V.A. Gutzeit, J. Ast, et al., Chem. Sci. 11 (2020) 7871–7883.
[41] I. Barasoain, J.F. Díaz, J.M. Andreu, Methods Cell Biol. 95 (2010) 353–372.
[42] G. Lukinavicius, L. Reymond, E. D'Este, et al., Nat. Methods 11 (2014) 731–733.
[43] G. Lukinavicius, G.Y. Mitronova, S. Schnorrenberg, et al., Chem. Sci. 9 (2018) 3324–3334.
[44] Z. Huang, R.P. Haugland, W. You, R.P. Haugland, Anal. Biochem. 200 (1992) 199–204.
[45] E. D'Este, D. Kamin, F. Gottfert, et al., Cell Rep. 10 (2015) 1246–1251.
[46] S. Karch, J. Broichhagen, J. Schneider, et al., J. Med. Chem. 61 (2018) 6121–6139.
[47] C.S. Chen, W.N.U. Chen, M. Zhou, et al., J. Biochem. Biophys. Methods 42 (2000) 137–151.
[48] M. Fan, H. An, C. Wang, et al., Chem. Eur. J. 27 (2021) 9620–9626.
[49] J. Ast, A. Arvaniti, N.H.F. Fine, et al., Nat. Commun. 11 (2020) 467.
[50] G. Lukinavicius, C. Blaukopf, E. Pershagen, et al., Nat. Commun. 6 (2015) 8497.
[51] J. Bucevicius, J. Keller-Findeisen, T. Gilat, et al., Chem. Sci. 10 (2019) 1962–1970.
[52] C. Spahn, J.B. Grimm, L.D. Lavis, et al., Nano Lett. 19 (2019) 500–505.
[53] K. Hiraoka, T. Inoue, R.D. Taylor, et al., Nat. Commun. 6 (2015) 6706.
[54] Y. Tsubono, Y. Kawamoto, T. Hidaka, et al., J. Am. Chem. Soc. 142 (2020) 17356–17363.
[55] R. Wirth, P. Gao, G.U. Nienhaus, et al., J. Am. Chem. Soc. 141 (2019) 7562–7571.
[56] R.S. Erdmann, H. Takakura, A.D. Thompson, et al., Angew. Chem. Int. Ed. 53 (2014) 10242–10246.
[57] A.D. Thompson, M.H. Omar, F. Rivera-Molina, et al., Angew. Chem. Int. Ed. 56 (2017) 10408–10412.
[58] L. Chu, J. Tyson, J.E. Shaw, et al., Nat. Commun. 11 (2020) 4271.
[59] A. Gupta, F. Rivera-Molina, Z. Xi, et al., Nat. Chem. Biol. 16 (2020) 408–414.